**Multimodal single-cell profiling of intrahepatic cholangiocarcinoma defines hyperactivated Tregs as a potential therapeutic target**

# Multimodal single-cell profiling of intrahepatic cholangiocarcinoma defines hyperactivated Tregs as a potential therapeutic target

Giorgia Alvisi 1, Alberto Termanini 2, Cristiana Soldani 3, Federica Portale 4, Roberta Carriero 2, Karolina Pilipow 1, Guido Costa 5, Michela Polidoro 3, Barbara Franceschini 3, Ines Malenica 3, Simone Puccio 6, Veronica Lise 7, Giovanni Galletti 1, Veronica Zanon 1, Federico Simone Colombo 8, Gabriele De Simone 8, Michele Tufano 1, Alessio Aghemo 9, Luca Di Tommaso 10, Clelia Peano 11, Javier Cibella 12, Matteo Iannacone 13, Rahul Roychoudhuri 14, Teresa Manzo 15, Matteo Donadon 5, Guido Torzilli 5, Paolo Kunderfranco 2, Diletta Di Mitri 16, Enrico Lugli 17, Ana Lleo 9

1Laboratory of Translational Immunology, IRCCS Humanitas Research Hospital, via Manzoni 56, 20089, Rozzano, Milan, Italy.

2Bioinformatics Unit, IRCCS Humanitas Research Hospital, via Manzoni 56, 20089, Rozzano, Milan, Italy.

3Laboratory of Hepatobiliary Immunopathology, IRCCS Humanitas Research Hospital, via Manzoni 56, 20089, Rozzano, Milan, Italy.

4Laboratory of Tumor Microenvironment, IRCCS Humanitas Research Hospital, via Manzoni 56, 20089, Rozzano, Milan, Italy.

5Humanitas University, Department of Biomedical Sciences, Via Rita Levi Montalcini 4, 20090 Pieve Emanuele - Milan, Italy; Division of Hepatobiliary and General Surgery, IRCCS Humanitas Research Hospital, via Manzoni 56, 20089, Rozzano, Milan, Italy.

6Laboratory of Translational Immunology, IRCCS Humanitas Research Hospital, via Manzoni 56, 20089, Rozzano, Milan, Italy; Institute of Genetic and Biomedical Research, UoS Milan, National Research Council, Rozzano, Milan, Italy.

7Laboratory of Translational Immunology, IRCCS Humanitas Research Hospital, via Manzoni 56, 20089, Rozzano, Milan, Italy; Humanitas University, Department of Biomedical Sciences, Via Rita Levi Montalcini 4, 20090 Pieve Emanuele - Milan, Italy.

8Flow Cytometry Core, IRCCS Humanitas Research Hospital, via Manzoni 56, 20089, Rozzano, Milan, Italy.

9Humanitas University, Department of Biomedical Sciences, Via Rita Levi Montalcini 4, 20090 Pieve Emanuele - Milan, Italy; Division of Internal Medicine and Hepatology, Department of Gastroenterology, IRCCS Humanitas Research Hospital, Rozzano, Milan, Italy.

10Humanitas University, Department of Biomedical Sciences, Via Rita Levi Montalcini 4, 20090 Pieve Emanuele - Milan, Italy; Department of Pathology, IRCCS Humanitas Research Hospital, via Manzoni 56, 20089, Rozzano, Milan, Italy.

11Institute of Genetic and Biomedical Research, UoS Milan, National Research Council, Rozzano, Milan, Italy; Genomic Unit, IRCCS Humanitas Research Hospital, via Manzoni 56, 20089, Rozzano, Milan, Italy; Human Technopole, Viale Rita Levi Montalcini 1, 20157, Milan, Italy.

12Genomic Unit, IRCCS Humanitas Research Hospital, via Manzoni 56, 20089, Rozzano, Milan, Italy.

13Division of Immunology, Transplantation and Infectious Diseases, IRCCS San Raffaele Scientific Institute, 20132 Milan, Italy; Vita-Salute San Raffaele University, 20132 Milan, Italy; Experimental Imaging Centre, IRCCS San Raffaele Scientific Institute, 20132 Milan, Italy.

14Department of Pathology, University of Cambridge, CB2 3QP, United Kingdom.

15Department of Experimental Oncology, European Institute of Oncology- IRCCS, Milan, Italy.

16Laboratory of Tumor Microenvironment, IRCCS Humanitas Research Hospital, via Manzoni 56, 20089, Rozzano, Milan, Italy; Humanitas University, Department of Biomedical Sciences, Via Rita Levi Montalcini 4, 20090 Pieve Emanuele - Milan, Italy.

17Laboratory of Translational Immunology, IRCCS Humanitas Research Hospital, via Manzoni 56, 20089, Rozzano, Milan, Italy. Electronic address: enrico.lugli@humanitasresearch.it.

**Background & Aims**

The landscape and function of the immune infiltrate of intrahepatic cholangiocarcinoma (iCCA), a rare, yet aggressive tumor of the biliary tract, remains poorly characterized, limiting development of successful immunotherapies. Herein, we aimed to define the molecular characteristics of tumor-infiltrating leukocytes with a special focus on CD4+ regulatory T cells (Tregs).

**Methods**

We used high-dimensional single-cell technologies to characterize the T-cell and myeloid compartments of iCCA tissues, comparing these with their tumor-free peritumoral and circulating counterparts. We further used genomics and cellular assays to define the iCCA-specific role of a novel transcription factor, mesenchyme homeobox 1 (MEOX1), in Treg biology.

**Results**

We found poor infiltration of putative tumor-specific CD39+ CD8+ T cells accompanied by abundant infiltration of hyperactivated CD4+ Tregs. Single-cell RNA-sequencing identified an altered network of transcription factors in iCCA-infiltrating compared to peritumoral T cells, suggesting reduced effector functions by tumor-infiltrating CD8+ T cells and enhanced immunosuppression by CD4+ Tregs. Specifically, we found that expression of MEOX1 was highly enriched in tumor-infiltrating Tregs, and demonstrated that MEOX1 overexpression is sufficient to reprogram circulating Tregs to acquire the transcriptional and epigenetic landscape of tumor-infiltrating Tregs. Accordingly, enrichment of the MEOX1-dependent gene program in Tregs was strongly associated with poor prognosis in a large cohort of patients with iCCA.

**Conclusions**

We observed abundant infiltration of hyperactivated CD4+ Tregs in iCCA tumors along with reduced CD8+ T-cell effector functions. Interfering with hyperactivated Tregs should be explored as an approach to enhance antitumor immunity in iCCA.

**Lay summary**

Immune cells have the potential to slow or halt the progression of tumors. However, some tumors, such as intrahepatic cholangiocarcinoma, are associated with very limited immune responses (and infiltration of cancer-targeting immune cells). Herein, we show that a specific population of regulatory T cells (a type of immune cell that actually suppresses the immune response) are hyperactivated in intrahepatic cholangiocarcinoma. Targeting these cells could enable cancer-targeting immune cells to act more effectively and should be looked at as a potential therapeutic approach to this aggressive cancer type.

**Introduction**

Cholangiocarcinoma (CCA) is a rare cancer that originates from the hepatobiliary epithelia and accounts for 3-5% of all gastrointestinal malignancies worldwide.1 Depending on the anatomic site of origin, CCA is divided into intrahepatic (iCCA), perihilar (pCCA), and distal (dCCA) CCA, with iCCA being the less prevalent type. However, the incidence rate of iCCA is constantly increasing and its mortality rate is extremely high, due to the aggressive evolution of the disease and the lack of efficient diagnostics and treatments.2 Late diagnosis highly compromises surgery, the only potentially curative option, and even among the 10-30% patients eligible for resection at diagnosis, 50% recur within the first year. Moreover, iCCA is a highly chemoresistant tumor, and pharmacological therapies are generally unsuccessful, with a 5-year survival rate that has persisted below 10% since the 1980s. Novel therapies targeting tumor subtypes with genetic rearrangements were introduced into clinical practice last year, following promising clinical trial results,3,4 but are only effective for 13-14% of patients based on their genomic alteration status.5,6 Therefore, there is an urgent need to develop valid therapeutic alternatives for iCCA.

During the last decade, immunotherapy approaches targeting checkpoint receptors expressed by tumor-infiltrating lymphocytes have revolutionized cancer treatment, increasing the overall survival (OS) of patients with multiple cancers.7,8 The superior responsiveness to anti-programmed-death (PD)-1 checkpoint inhibitors is thought to be mediated by the unleashed reactivity of clonally expanded CD8+ T cells towards the cognate tumor antigens,9,10 among which those that are less differentiated, or stem-like, are endowed with enhanced functionality and capability for long-term persistence.[11], [12], [13], [14] In this regard, tumors with high mutational burden respond better to checkpoint-inhibitor therapy.15 Accordingly, tumors with mismatch repair deficiency and consequently high DNA microsatellite instability are highly responsive to anti-programmed cell death 1 (PD-1) treatment.16 In this context, the FDA approved the use of an anti-PD-1 antibody in 2017 in CCA and other solid tumors with microsatellite instability or mismatch repair deficiency, which nevertheless benefits only a small proportion of patients with iCCA.17,18

The tumor microenvironment is infiltrated by a diverse population of immune cells, among which effector and cytotoxic T cells and natural killer (NK) cells mediate tumor immunosurveillance. By contrast, inhibitory subpopulations, including CD4+ regulatory T cells (Tregs) and tumor-associated myeloid cells, can counteract immune responses and favor tumor growth.19 Several studies have recently deciphered the architecture of the tumor microenvironment of several cancers, expanding our knowledge of its complex composition and revealing novel drug targets. Such analyses now begin to reveal that many immune lineages are not compartmentalised into discrete subcompartments but, rather, comprise a continuum of functional phenotypes.

Knowledge regarding the complexity of the immune system in iCCA is still limited. Overall, iCCA is poorly infiltrated by the immune system, and is generally referred to as a “cold” tumor.

Immunohistochemical analysis initially revealed the preferential presence of CD8+ and CD4+ T cells in tumors and in peritumoral areas, respectively.20 A subsequent study in a cohort of 306 individuals with biliary tract cancers revealed that longer OS correlated positively with a higher tumor infiltration of total CD4+ tumor-infiltrating lymphocytes, but did not distinguish CD4+ T-cell subtypes.21 A recent study using single-cell RNA-sequencing (scRNA-seq) of tumoral and peritumoral samples elucidated at least in part the landscape and gene expression of cells infiltrating iCCA, revealing the presence of activated Tregs, T cells expressing inhibitory receptors and a diverse population of cancer-associated fibroblasts. Among these, a predominant subpopulation of CD146+ vascular cancer-associated fibroblasts expressed high levels of IL-6, which in turn promoted tumor progression via IL-6R signaling on malignant cells.22 Even though the architecture of the immune system infiltrating iCCA is starting to be appreciated,[22], [23], [24] the regulation and functionality of specific immune populations regulating the antitumor immune response are still poorly characterized.

## Materials and methods

### Study design

Experiments were approved by the Humanitas Research Hospital Institutional Review Board (approval no. 146/20 for patients' samples and no. 28/01/2016 for buffy coats from healthy donors) and were conducted in accordance with the Declaration of Helsinki. All patients were enrolled at Humanitas Research Hospital and provided informed consent for tissue biobanking. All patients had pathology proven iCCA and were without chemotherapy treatment prior to resection. Hepatitis B- or C-positive patients, as well as those with cirrhosis, were excluded. Samples (one tumoral and one peritumoral) were selected from areas without macroscopic evidence of necrosis or hemorrhage. For morphological analysis, sections were cut (2 μm thick), stained with H&E and evaluated by an expert liver pathologist. The histological features that were evaluated included tumor grade, desmoplasia, resection margin, steatosis, perineural, and lymphovascular invasion, and lymph node metastasis. Patients with resected iCCA were followed up every 3 months, as per protocol in our center, or until death, and major events were recorded. Characteristics of the patients enrolled in the study are listed in Table S1.

### Sample collection and processing

Peripheral blood mononuclear cells (PBMCs) were isolated from buffy coats from patients with iCCA and healthy donors via density-gradient separation and were cryopreserved in FBS supplemented with 10% DMSO until use. Blood samples from patients were collected in vacutainer EDTA Tubes (BD). Tissues were collected in complete R10 medium: RPMI-1640 medium with 10% FBS (Sigma-Aldrich), 1% penicillin-streptomycin and 1% Ultra-glutamine (both from Lonza). Human cell isolation from healthy liver was performed by collagenase perfusion, adapting a traditional 2-step technique.48 Briefly, non-tumoral tissue displaying the normal vascular architecture was perfused in order to collect the circulating intrahepatic blood (perfusate). Then, the liver sample was digested with collagenase, obtaining a single-cell suspension. Parenchymal cells eliminated from the sample through appropriate centrifugations were counted, then stored. Cells were pelleted, counted, and frozen according to the slow freezing procedure in standard cryo-vials. Further disaggregation of iCCA tissue into a single-cell solution for sequencing was completed using the MACS tumor dissociation kit (Miltenyi Biotec) with the standard tough tumor protocol. Briefly, the MACS tumor dissociation kit enzyme mix (300 μl) was added to each sample. Next, samples were put into the gentleMACS Dissociator and ran through the tough tumor program. The cell suspension was then applied to a 70 μm cell strainer. Cells were pelleted, counted and frozen according to the slow freezing procedure in standard cryo-vials (1 ml cell suspension in the cryopreservation medium as above).

Polychromatic flow cytometry

Frozen samples were thawed in R10 additioned with 20 µg/ml DNase I from bovine pancreas (Sigma-Aldrich). After washing with PBS (Sigma-Aldrich), the cells were stained with a combination of monoclonal antibodies chosen arbitrarily on the basis of current knowledge about tumor-infiltrating leukocytes and listed in Table S2. Flow cytometry procedures for (i) selection of antigen-fluorochrome combinations, (ii) reagent titration and validation, and (iii) limiting spreading error have been described previously.25 Flow cytometry data were analyzed on a FACS Symphony A5 cytometer (BD Biosciences) equipped with 5 lasers (UV, 350 nm; violet, 405 nm; blue, 488 nm; yellow/green, 561 nm; red, 640 nm; all tuned at 100 mW, except for UV, tuned at 60 mW). Compensation was performed by FlowJo using BD Compbeads incubated with single antibodies, as previously described.49 The cohorts of patients with non-small cell lung cancer (NSCLC), breast cancer (BC) and colorectal cancer (CRC) used to assess CD39 expression by tumor-infiltrating CD8+ T cells have been described previously.28,32,50

For further details regarding the materials and methods used, please refer to the CTAT table and supplementary information.

**Results**

High-dimensional flow cytometry defines the T-cell and myeloid cell composition of human iCCA

We initially generated single-cell suspensions from the tumor and the adjacent tumor-free tissue (hereafter referred to as peritumor), and isolated PBMCs from 20 patients eligible for surgery after diagnosis (Table S1). In addition, we isolated circulating immune cells that are abundant in the liver parenchyma by organ perfusion (hereafter referred to as perfusate). We next profiled single cells with 2 high-dimensional flow cytometry panels25 encompassing markers of T-cell memory and effector differentiation, activation, cytotoxicity and exhaustion, CD4+ Treg markers, as well as markers related to subsets of myeloid cells (Fig. 1A and Table S2). CD3+ cells, identifying the bulk of T cells, and CD3– CD66b– cells, enriching mainly for myeloid cells, were further analyzed by PhenoGraph, a computational algorithm capable of clustering single cells according to their relative expression of antigens in the multidimensional space. In this way, we identified 7, 10 and 12 CD4+, CD8+ and myeloid clusters, respectively (Fig. 1B), whose profile of antigen expression is shown in the heatmaps in Fig. S1A and S4A. Representative flow cytometry profiles of major T-cell and myeloid subsets identified by PhenoGraph are shown in Fig. S2 and S5, respectively.

Principal component analysis of PhenoGraph cluster abundance revealed that the 4 tissue sites had a different T-cell and myeloid composition as a whole, although perfusate and the peritumor tended to share a similar T-cell immunophenotypic landscape (Fig. 1C). Specifically, PBMCs were characterized by the presence of CD4+ naïve and memory T cells expressing C-C chemokine receptor 4 (labelled as CD4+ CCR4+), CD45RO+ CCR7+ central memory CD8+ T cells (CD8+ TCM) as well as CD9+ and CD9– classical monocytes bearing a CD14+CD16– phenotype. Perfusate and peritumor mainly displayed CD4+ granzyme K+ CCR2dull (CD4+ GZMK+), CD8+ T cells with a CD45RO– CCR7– GZMK+ GZMB+ phenotype (CD8+ CTL.2) and CD8+ T cells with a CD127high GZMK+ CD161+ phenotype (preferentially including mucosal associated invariant T [MAIT] cells). Myeloid cells present in these tissues displayed a CD11b+ phenotype expressing or not CD11c, or a CD11b+CD11c+ HLA-DRhigh CD141+ phenotype, suggesting the presence of immature myeloid cells and conventional type 1 dendritic cells (cDC1), respectively. Tumors mainly displayed subsets of CD4+ and CD8+ memory T cells expressing different combinations of CD69 and CD103, collectively labelled as tissue-resident memory T cells (TRM; Fig. 1C,D and Fig. S1B-C). In the case of CD8+ T cells, a subset of CD69+ CD103+ TRM also expressed high levels of CD39 (CD8 TRM CD39+) (Fig. 1D), a marker recently associated with CD8+ T-cell reactivity to tumor antigens.26,27 In line with their putative chronic stimulation by antigens, these cells also expressed increased levels of the inhibitory receptor PD-1 and the activation marker CD38 compared to other iCCA-infiltrating CD8+ T-cell clusters (Fig. S1A). Albeit being present almost exclusively in

tumors, the frequency of CD8+ CD39+ TRM was low (median = 0.68, IQR: 0.41 and 3.32; Fig. 1D) and comparable to that found in BC.28 By contrast, NSCLC and CRC lesions displayed a much higher frequency of these cells (Fig. S3A, B). Overall, these data confirm the poor immunogenicity of human iCCA or suppression of T-cell responses against them.

Notably, tumors were highly infiltrated by CD4+ CD127– CD25+ Tregs (Fig. 1C-E; Fig. S1A) overexpressing PD-1, CD39, CCR8, CD69 and the transcription factor (TF) T-bet compared to Tregs from other tissue sites or the circulation (Fig. 1F and Fig. S3C). We confirmed FOXP3 expression by virtually all of these cells from a subset of patients (n = 5; Fig. S3D) and further identified 2 major subclusters of Tregs by PhenoGraph analysis, according to which "activated" Tregs more frequently expressed the effector Treg-related markers 41BB, ICOS, CCR8, GITR and, to a lesser extent, PD-L1 compared to "quiescent" Tregs (Fig. S3D, E). Overall, these data confirm that iCCA-infiltrating Tregs show a heterogeneous pattern and activated phenotype similar to those previously found in other solid tumors.[29], [30], [31], [32] As far as myeloid cells were concerned, tumors were preferentially infiltrated compared to other tissues by CD11b+ CD11c+ HLA-DRhigh CD1c+ conventional type 2 dendritic cells (cDC2) (Fig. 1D), and by CD11b– CD9+ cells. Tumors were also infiltrated by CD11c– HLA-DRhigh CD123+ plasmacytoid DCs, which were also abundant in the perfusate and in the peritumoral area, less so in the PBMCs, and by CD11b+ CD11c+ immature myeloid cells, which instead were ubiquitous (Fig. 1C-D; Fig. S4A, B). Overall, these data indicate that human iCCA is characterized by a different landscape of T-cell and, to a lesser extent, myeloid phenotypes compared to peritumoral and circulating sites.

**scRNA-seq reveals tumor-specific differences in gene expression by specific T-cell subpopulations**

We next performed scRNA-seq of CD45+ immune cells isolated from 6 iCCA and paired peritumoral tissues to gain more insights on the molecular characteristics of the tumor-specific immune infiltrate (Fig. 2A; see Table S1 for the characteristics of the patients included in this experiment). Cluster analysis of scRNA-seq data and subsequent enrichment of defined immune signatures revealed that, among immune cells, T and NK cells were most abundant, followed by myeloid cells and B cells (Fig. 2B and Fig. S6A,B). CD45– stromal/tumor cells from 2 patients, spiked in at known concentration as a control, separated from these subsets of immune cells. Among CD45+ cells, tumors tended to harbor increased frequencies of T cells, reduced frequencies of NK and B cells, and similar frequency of myeloid cells compared to adjacent peritumoral tissue (Fig. S6B). Overall, tumoral and peritumoral tissues could be clearly distinguished on the basis of T- and NK cell gene expression profiles, and less so by B-cell and myeloid profiles, indicating that T cells and NK cells undergo specific transcriptional changes in the tumor (Fig. S6C). Inspired by flow cytometry results, we focused our subsequent investigation on T cells and myeloid cells, and subclustered these populations of cells to further identify their transcriptional characteristics within tumors compared to the adjacent peritumoral tissue. We identified 8 clusters of myeloid and 11 clusters of T cells, reflecting, at least in part, those subpopulations that were identified by flow cytometry. The frequency of these clusters in peritumoral and tumoral samples from individual patients is shown in Fig. S6D.

As scRNA-seq datasets may be characterized by zeros and dropout events, we employed imputation of single-cell data, a computational approach capable of inferring gene expression even in the presence of dropouts, to improve the detection of gene expression (see supplementary methods). For instance, this approach improved the detection of CD4 and CD8A mRNA expression (Fig. S7A). Among myeloid cells, we identified CD14high classical monocytes (C0) expressing S100A8, VCAN and CD36, among other genes; ID3high macrophages (C1) expressing VSIG4 and resembling tissue-resident

Kupffer cells, as previously suggested;33 MARCOhigh macrophages (C3) expressing PLIN2, APOC1 and SPP1, among others; TREM2high macrophages (C5) expressing APOC1 and C1QA/B/C; cDC2 (C2), expressing FCER1A, ADAM8, CD1C, CLEC10A and IRF4; cDC1 (C7), expressing IRF8, IDO1, CLEC9A and BATF3; and non-classical monocytes (C6) expressing FCGR3A, CDKN1C, LILRA1 and LILRB2.34 Among T cells, we identified subsets of early differentiated memory T cells (C2, C5 and C8), expressing different combinations of genes previously related to stem-like memory cell differentiation such as CCR7, GPR183, IL6R, SATB1, CCR4 and IL7R;35 subsets of effector cells (C0, C3, C6 and C7), expressing different combinations of genes previously related to effector memory differentiation, such as CSF1 (encoding M-CSF), TNF, IFNG, TBX21 [encoding the TF T-bet], ID2, PRDM1 (encoding the TF BLIMP-1), GZMA, GZMK and the C-C chemokines CCL4 and CCL5, among others; a terminally differentiated/cytotoxic subset (C1), expressing the cytotoxicity-related genes CRTAM, NKG7 and PRF1 (encoding perforin) and the terminal differentiation-related TF ZEB2; a TRM cell subset (C4), expressing ITGAE (encoding CD103 integrin), CISH, CCR2, HOPX as well as detectable levels of ENTPD1 (encoding CD39), suggesting potential tumor reactivity26,27 (Fig. 2D and Fig. S7B); and a subset expressing several CD4+ Treg-related genes (C10), including IL2RA, FOXP3, BATF, TIGIT, CD177, IL1R2, among others (Fig. 2D). An additional subset, C9, was found to express CCL20, IL23R, RORC and KLRB1 (encoding CD161), suggesting the identification of CD8+ MAIT cells or, alternatively, CD4+ T helper type-17 cells (Th17). The poor expression of CD4 and CD8A by C9 (Fig. S7A) precluded further distinction between these 2 subsets.

Overall, scRNA-seq revealed increased abundance of MARCOhigh myeloid cells and of CD4+ Tregs in tumoral compared to peritumoral tissues (Fig. 2E), in line with results obtained by flow cytometry, although it could not detect additional differences, likely due to the limited number of patients that could be analyzed using scRNA-seq. Nevertheless, scRNA-seq identified differences in T-cell gene expression between these 2 sites (Fig. S7B). This was most evident for C4 TRM and C7 effector subsets from tumors, in which HAVCR2 (encoding the inhibitory receptor TIM-3) and CTLA4 (only C7) were upregulated and effector/killer molecules were downregulated compared to those from peritumoral tissue (Fig. S7B,C). The biggest differences were observed among Tregs, where those from tumors upregulated CTLA4, HAVCR2, TIGIT, BTLA and ENTPD1 (Fig. S7B), among others (Fig. S7C and Table S3). This iCCA-infiltrating Treg gene signature was significantly enriched in an independent dataset of bulk RNA-seq obtained by comparing iCCA vs. the peritumor (Fig. S7D).6 Similar data were obtained with a gene signature obtained by comparing highly immunosuppressive, intratumoral ICOS+ CCR8+ Tregs vs. more quiescent ICOS– CCR8– Tregs.32 Overall, these data suggest functional modulation of the iCCA T-cell infiltrate, with heightened activation of Tregs and reduced functional capacity of putative tumor-specific ENTPD1high TRM cells and effector T cells.

**Dynamic remodeling of the Treg interactome in iCCA**

Inspired by the modulation of Treg ligands and receptors in tumoral vs. peritumoral tissues, we then investigated the molecular identity of Treg interactions with the surrounding microenvironment by using CellPhoneDB, a computational algorithm capable of predicting cell-cell communications from differentially expressed ligand:receptor (L:R) pairs in single-cell data (see Methods). We found that, overall, Tregs interacted with different T-cell and myeloid subsets via multiple de novo interactions, or via interactions that were more significant in tumors vs. peritumors. The repertoire of these interactions, that involved co-inhibitory and co-stimulatory signals, TNF superfamily members, cytokines, chemokines and their receptors, tended to be different among T-cell clusters, while relatively uniform among myeloid clusters (Fig. 3A, B). Among others, we found enhanced interactions between CD80 and CD86 expressed by myeloid cells and the CD28 co-stimulatory receptor expressed by Tregs. Similarly, the TNF superfamily members CD70 and TNFSF4 (encoding OX-40 ligand), overexpressed by T-cell subsets, and TNFSF9, encoding 41BB ligand and expressed by both T and

myeloid cells, interacted with their cognate receptors CD27, TNFRSF4 (OX-40) and TNFRSF9 (41BB) in tumors, suggesting that these interactions are important for the maintenance of activated Tregs as recently shown in murine models.37 Importantly, CD80 and CD86 also showed enhanced predicted interaction with CTLA4, highly expressed by Tregs in tumors and important for the Treg-mediated inhibition of immune responses via competition with CD28. Additional interactions of note that were stronger in tumors vs. peritumors involved CD200 and SIRPG inhibitory ligands expressed by intratumoral Tregs interacting with CD200R1 and CD47 expressed by myeloid cells, respectively. Both of these interactions are possibly involved in the downregulation of inflammatory responses. Thus, iCCA-infiltrating Tregs are characterized by extensive remodeling of the expression of receptor ligand pairs required for cell-cell communication, suggestive of enhanced Treg-mediated immunosuppression in the iCCA microenvironment.

**Transcriptional network inference to understand the molecular basis of diminished effector T-cell activation and enhanced Treg activation in iCCA**

Co-regulation of TFs defines cell fate and functional responses. To better understand TF networks regulating iCCA-infiltrating T cells, we applied SCENIC, a computational algorithm capable of predicting TF activity via the analysis of binding motifs that are enriched at the promoters of expressed genes in scRNA-seq data (see methods) (Fig. 4A). SCENIC analysis clearly separated tumoral and peritumoral T cells (Fig. 4A) as well as the majority of T-cell clusters defined by scRNA-seq (Fig. 4B), thus indicating that tissue-derived T-cell states can be described by their inferred TF activity. Among others, we found that IRF2, IRF3 and STAT1-mediated transcriptional activities, possibly dependent on type I interferon signaling and involved in promoting effector functional capacity,38 were reduced in tumoral vs. peritumoral T-cell clusters, especially in C3, C6 and C7 of effector cells and, to a lesser extent, in C4 of TRM cells (Fig. 4B). C7 along with C1 of terminal/cytotoxic T cells from tumors vs. peritumors also showed reduced transcriptional activities of RUNX3, EOMES and TBX21 TFs, which mediate the expression of effector and cytotoxic molecules. Altogether, these data suggest loss of TRM and effector T-cell functionality in iCCA is due to altered, cell type-specific transcriptional programs. By contrast, tumor-infiltrating Tregs displayed increased activity of several TFs compared to those infiltrating the peritumor, including FOXP3, the lineage-specification factor for Treg cells; IKZF2, linked to stability of the Treg lineage;39 IRF4 and its transcriptional partner BATF, recently reported to promote Treg activation and suppressive activity in tumors;32 STAT5A and SMAD1, possibly reflecting IL-2 and TGF-β signaling, respectively; and several others, such as VDR, SOX9, ZEB1 and MEOX1, whose function in Treg biology remains poorly characterized (Fig. 4B).

We next ordered TF activities in pseudo-time by using a dedicated algorithm, i.e. SCORPIUS (see Methods), to possibly identify specific patterns of their activation or repression during Treg differentiation from peritumors to tumors. In line with data at the level of single genes, SCORPIUS was able to clearly separate Tregs from the 2 different sites (Fig. 4C), and identified clusters of activity (Fig. 4D), suggesting that different TFs might be involved at different steps of Treg hyperactivation in iCCA. Specifically, loss of activity of FLI1, recently shown to inhibit effector CD8+ T-cell differentiation in murine models of chronic infection and cancer,40 was accompanied by increased activity of several TFs simultaneously, e.g., of IKZF2, SMAD1, VDR, IRF4, FOXP3 and BATF, during transition from peritumors to tumors. We also revealed increased activity related to EZH2, a histone H3K27 methyltransferase elevated in tumor-infiltrating Tregs and whose pharmacological inhibition results in proinflammatory Treg reprogramming and enhanced antitumor immunity.41,42 A second group of TFs, including MEOX1, TP73 (encoding p73), SOX9 and FOXA1, among others, was activated transiently in

Tregs in iCCA, and was later followed by enhanced ZMIZ1 and MYB activities (Fig. 4D). Collectively, our analysis identified novel TF activities possibly related to hyperactivated Treg differentiation and enhanced immune suppression in iCCA.

**MEOX1 transcriptionally and epigenetically reprograms circulating Tregs to a tumor-infiltrating phenotype**

We next focused our investigation on one of the top hits from SCENIC analysis of intratumoral Tregs, i.e., MEOX1, whose role in the immune system is unknown. MEOX1 encodes a mesodermal TF that plays a key role in somitogenesis and sclerotome development and whose mutation in humans results in the incomplete development of bones in the neck (also known as Klippel-Feil syndrome).43 MEOX1 mRNA levels strongly correlated with those of FOXP3 in the cholangiocarcinoma dataset from the cancer genome atlas (Fig. S8A), suggesting a relationship with Tregs in tumors. In our scRNA-seq dataset, MEOX1 expression could be detected only in tumor-infiltrating Tregs, and not in other infiltrating CD4+ or CD8+ T cells (Fig. S8B, C). A similar trend of expression could be observed in a second scRNA-seq dataset of iCCA that was recently published (Fig. S8D).22 Also, Tregs from lung, ovarian and breast tumors significantly overexpressed MEOX1 compared to conventional CD4+ T cells (Tconv; Fig. S8E). By analyzing the MEOX1 promoter, we found binding motifs of FOXP3, IRF4, FOXO1, EZH2 and IKZF2 TFs, among others (Fig. 5A). Moreover, the predicted activity of these TFs was co-regulated with that of MEOX1 in a subset of iCCA-infiltrating Tregs (Fig. 5B), collectively suggesting a role in the regulation of MEOX1 expression. To investigate the functional importance of MEOX1 in specifying the molecular characteristics of tumor-infiltrating Tregs, we isolated peripheral blood CD4+ Tregs from healthy donors, activated them for 24 hours with anti-CD3/28 + IL-2 and transduced them with a lentivirus capable of overexpressing the full-length MEOX1 cDNA, or with a mock lentivirus control. Transduced cells, identified by the GFP reporter, were further purified as CD127– CD25+ by FACS (Fig. S9A) and analyzed at the transcriptomic and chromatin accessibility level by bulk RNA-seq and assay for transposase-accessible chromatin using sequencing (ATAC-seq), respectively (Fig. 5C). At the chromatin level, we found that genes previously shown to be overexpressed by Tregs in tumors and associated with effector differentiation (TNFRSF9, IL1RN)32 and with disease progression in multiple cancers (LAYN),30 or responsible for IL-10 production by Tregs (PRDM1),44 among others (Table S7), were more accessible at multiple genomic sites in MEOX1-transduced vs. mock-transduced Tregs (Fig. 5D). Computational analysis of differentially accessible regions in the whole ATAC-seq dataset further identified differentially accessible TF-binding motifs. Motifs attributable to AP-1 (FOS, JUNB and the combined FOS:JUNB motif), to AP-1 transcriptional partners (BATF, IRF4 and the combined BATF:JUN motifs, mechanistically linked to hyperactivated Tregs in tumors)32,45 and the SMAD2:SMAD3 combined motif, reflecting increased accessibility of genes possibly controlled by TGF-β signaling, were enriched in MEOX1-transduced Tregs, whereas motifs attributable to TWIST2, MXI1, KLF9 and TP53 were enriched in mock-transduced Tregs (Fig. 5E). In agreement with ATAC-seq results, overexpression of MEOX1 upregulated the effector Treg-related genes TNFRSF9, IL1RN, LAYN, CD70, MAGEH1, ICOS, NRP1 (encoding Neuropilin-1), IL10 and CTLA4 (Fig. 5F). By gene set enrichment analysis, MEOX1-overexpressing Tregs were strongly enriched in specific transcriptomic signatures of Treg vs. CD4+ Tconv, of iCCA vs. peritumor-infiltrating Tregs (Table S3), or of ICOS+ CCR8+ vs. ICOS– CCR8– Tregs (Fig. 5G).32 Thus, MEOX1 promotes the acquisition of a tumor-infiltrating Treg phenotype by reprogramming the transcriptional and epigenetic landscape of circulating Tregs.

**Suppressive potential and prognostic significance of MEOX1-expressing Tregs**

We next investigated the role of MEOX1 in shaping the functional capacity of Tregs. Circulating Tregs overexpressing MEOX1 tended to be more efficient than mock-transduced Tregs at inhibiting proliferation (assessed by CTV dilution) and activation (CD25 expression) of CD4+ Tconv treated with anti-CD3/28 in vitro, especially at a Tconv:Treg ratio of 4:1 (Fig. 6A,B). MEOX1 overexpression also resulted in increased surface levels of 41BB and, to a lesser extent, CTLA4 following TCR restimulation of Tregs at day 4 after transduction (Fig. 6C,D), thereby confirming previous data showing that TNFRSF9 and CTLA4 are also MEOX1 targets at the protein level. Considering the negative prognostic impact of these and other Treg-related genes in multiple cancers,[30], [31], [32] we tested whether the gene program induced by MEOX1 in Tregs (Table S9) could specifically influence iCCA disease progression as determined by signature enrichment in a large cohort of treatment-naïve tumors previously characterized by bulk RNA-seq.36 Given the clinical diversity of the 2 cohorts, patients with HBV positivity, elevated AFP, and liver fluke were excluded from the analysis; out of 244 reported patients, 147 were included in the analysis. When related to the content of CD8+ T cells, which is generally associated with favorable prognosis, MEOX1-dependent gene program enrichment was significantly associated with worse OS, both in univariate (Fig. 6E) and in multivariate analysis after correction for co-varying factors such as the presence of intrahepatic metastasis, regional lymph node metastasis, distal metastasis and preoperative CA 19-9 levels (Fig. 6F and Fig. S9B). We obtained very similar results when relating the MEOX1-dependent gene program to a cDC2 signature (Fig. 6E, F), in accordance with recent data showing Treg-dependent inhibition of cDC2 activity and tumor immunosuppression in other cancers.46 Overall, our data identify MEOX1-dependent Treg crosstalk in the iCCA microenvironment, the disruption of which might favor antitumor immune responses.

## Discussion

We provide a comprehensive characterization of T-cell and myeloid subsets that are present in patients with iCCA using high-dimensional single-cell technologies. We identified extensive tumor infiltration of CD4+ Tregs with a hyperactivated and highly immunosuppressive phenotype, which is accompanied by the loss of CD8+ cytotoxic T-lymphocytes. CD8+ T cells expressing CD39, a marker recently linked to the identification of tumor-specific CD8+ T cells in the tumor microenvironment, represented only a minor fraction of CD8+ T cells in iCCA. The abundance of CD39+ CD8+ T cells is much lower than that reported for highly immunogenic tumors, such as NSCLC, CRC (this paper) and melanoma.27 This observation reinforces previous evidence that, overall, iCCA is poorly immunogenic, thereby contributing to explain, among other factors, its low response to checkpoint blockade with anti-PD-1.17,18 It is curious to note that a few patients in our cohort harbored a very high frequency of CD39+ CD8+ T cells, leading us to speculate that a particular set of tumor (neo)antigens are potentially expressed in the microenvironment. By contrast, changes at the level of the myeloid compartment were less evident and were mainly ascribed to the increased infiltration of cDC2, rather than to changes in overall gene expression, compared to other tissue sites.

scRNA-seq further informed on the characteristics of the different immune cell types and enabled the identification of a major suppressive hub orchestrated by Tregs in the iCCA tumor microenvironment. Compared to the adjacent peritumoral tissues, iCCA-infiltrating Tregs showed features of the hyperactivated effector state previously described in several solid tumors, including melanoma, NSCLC, hepatocellular carcinoma, renal cancer, BC and CRC.[29], [30], [31], [32] Although differences that are yet to be identified might be present according to the specific tumor type, it seems evident that intratumoral Tregs share a core transcriptional and functional program, characterized by the

increased expression of inhibitory molecules, chronic immune activation and enhanced suppressive capacity compared to those from the circulation or the peritumoral area. Tregs are predicted to engage multiple inhibitory pathways on T and myeloid cells in the tumor microenvironment, while receiving signals that in turn may support their hyperactivated phenotype, thereby offering novel, more specific targets for cancer immunotherapy. In agreement with the Treg-mediated inhibition, in several iCCA-infiltrating T-cell subsets we observed reduced activity of TFs promoting the cytotoxic program and effector function of T cells, including RUNX3, EOMES and TBX21 (encoding T-bet) activities. We still do not know what the relationship between enforced surface interactions and altered downstream gene expression/TF activities in T cells in iCCA is. We anticipate that the future development of computational tools capable of integrating multiple layers of information, including at the level of single cells, will identify with precision those regulatory circuits that should be targeted to interfere with specific dysfunctional programs.

Among infiltrating T cells, Tregs had the most diverse molecular program compared to those present in the adjacent peritumoral tissue, corroborating the hypothesis that these cells play a central role in orchestrating immunosuppression in iCCA. We identified several TFs whose enhanced activity has previously been shown to regulate immune activation of Tregs in solid tumors. These included IRF4, BATF and EZH2, which play an essential role in suppression of antitumor immunity,32,41,42 in addition to TFs whose functional role in Treg biology remains to be established. Among these, we found that overexpression of MEOX1 was sufficient to reprogram circulating Tregs to acquire a transcriptional and epigenetic landscape that is highly reminiscent of tumor-infiltrating Tregs, and to induce 41BB and CTLA4 expression, which are predicted to engage their cognate ligands on several T-cell and myeloid populations in the tumor microenvironment. We acknowledge that employment of circulating Tregs activated in vitro to assess MEOX1 function could represent a limitation, as these cells might only reflect part of the molecular landscape of tumor-infiltrating Tregs. This experimental strategy could explain the only modest increase in the ability to suppress Tconv proliferation when MEOX1 is ectopically overexpressed. Nevertheless, the gene program downstream of MEOX1 strongly correlated with worse OS specifically in iCCA, leading us to hypothesize that additional signals in the tumor microenvironment are required to shape and further sustain the inhibitory potential of Tregs. The mechanisms by which MEOX1 is induced and operates in hyperactivated Tregs remains to be established. MEOX1 is triggered by TGF-β signaling in non-immune cells such as cardiac fibroblasts,47 and mediates cell differentiation by direct binding to DNA. Although these aspects were not tested directly on intratumoral Tregs, pseudotemporal ordering of TF activities and molecular analyses inspire a model according to which IRF4 and BATF precede MEOX1 activity, which in turn sustains hyperactivated Treg gene expression by favoring chromatin accessibility at AP-1/IRF4/BATF consensus sites.

In conclusion, we provide a comprehensive characterization of the iCCA T-cell and myeloid infiltrate and show that Treg abundantly infiltrate the tumor microenvironment while cytotoxic T lymphocytes and CD39+, putative tumor-specific CD8+ T cells expressing PD-1 are rare. Future immunotherapeutic strategies must thus aim to turn iCCA from cold to hot, so to favor T-cell infiltration. Interfering with the hyperactivated Treg program, such as that regulated by MEOX1, which is shared by several solid tumors, seems an attractive approach to consider in this regard.

**Abbreviations**

ATAC-seq, assay for transposase-accessible chromatin using sequencing; cDC1/2, conventional type 1/2 dendritic cells; iCCA, intrahepatic cholangiocarinoma; MAIT, mucosal-associated invariant T; MEOX1, mesenchyme homeobox 1; PD-1, programmed cell death-1; scRNA-seq, single-cell RNA-sequencing; Tconv, conventional T cell; TF, transcription factor; Treg, regulatory CD4+ T cell; TRM, tissue-resident memory T cell.

**Financial support**

This work was funded by the Associazione Italiana per la Ricerca sul Cancro (AIRC IG 2017 – ID 20676 to E.L. and AIRC IG 2019 – ID 23408 to A.L.). G.G. and S.P. were supported by Fellowships from the Fondazione Italiana per la Ricerca sul Cancro-Associazione Italiana per la Ricerca sul Cancro (FIRC-AIRC). K.P. is a recipient of the Fondazione Umberto Veronesi 2020 postdoctoral fellowship. D.D.M was supported by Associazione Italiana per la Ricerca sul Cancro (AIRC Start up 19141 and AIRC 5x1000 2019-ID 22757) and Minsal (GR-2016-02363531). M.I. was supported by the European Research Council (ERC) Consolidator Grant 725038, ERC Proof of Concept Grant 957502, Associazione Italiana per la Ricerca sul Cancro (AIRC) Grants 19891 and 22737, Italian Ministry of Health (MoH) Grants RF-2018-12365801, and Funded Research Agreement from Gilead Sciences, Asher Bio, Takis Biotech and Vir Biotechnology. The purchase of a FACSSymphony A5 was defrayed in part by a grant from the Italian Ministry of Health (Agreement 82/2015).

**Authors' contributions**

Conceptualization and design of study (GA, AT, CS, PK, DDM, EL, AL). Data generation (GA, AT, FP, RC, KP, GC, SP, VL, GG, MT, CP, JC, PK). Sample collection and processing (CS, MP, BF, IM, VZ, FSC, GDS, AA, LDT, TM, MD, GT). Single-cell data analysis (GA, AT, SP, PK). Data analysis and interpretation (GA, AT, FP, RC, SP, MI, RR, PK, DDM, EL, AL). Manuscript preparation (GA, AT, DDM, EL, AL). Critical review and editing (all authors). Funding (DDM, EL, AL).

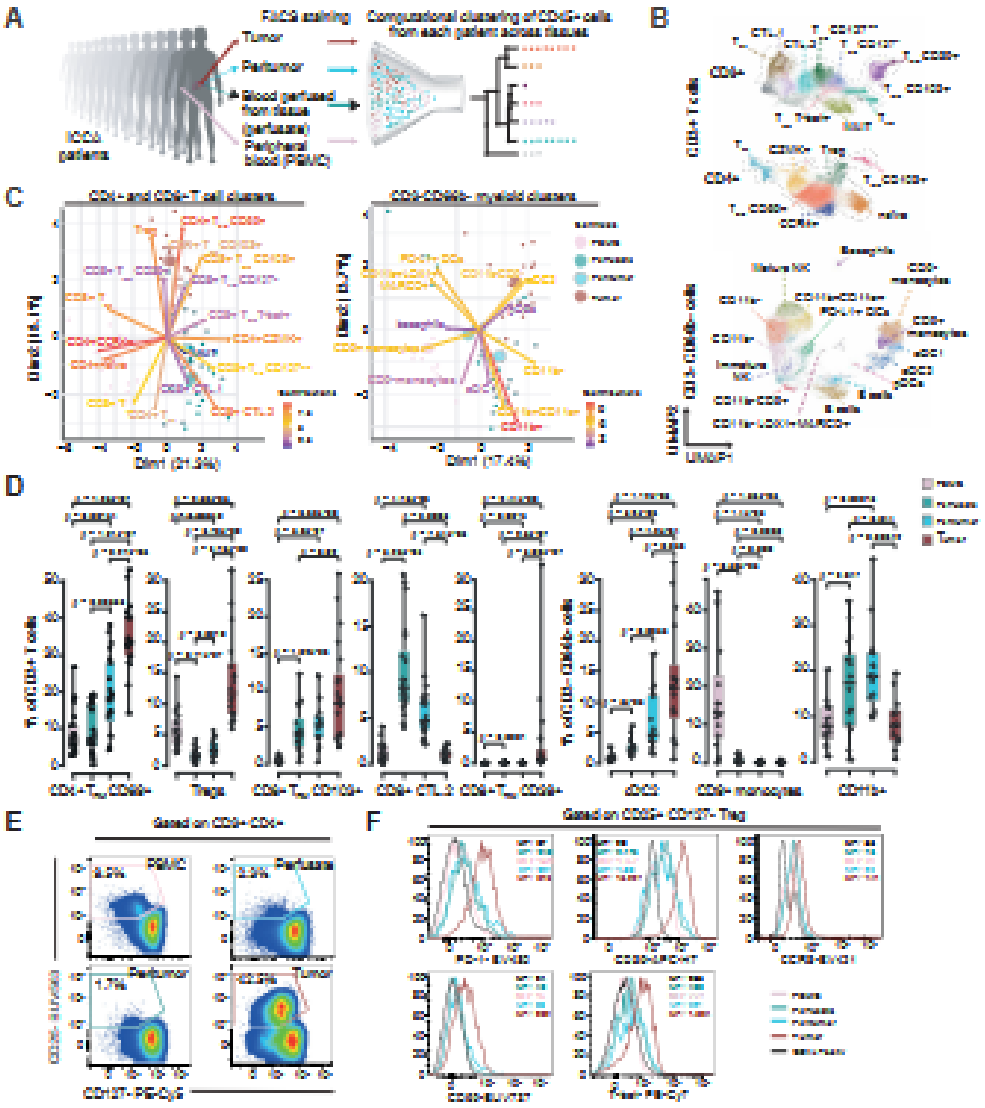


Fig. 1. Single-cell profiling of CD45+ cells in human iCCA. (A) Experimental workflow. (B) UMAP of PhenoGraph clusters from flow cytometry of tissues (T cells:

n = 20; myeloid: n = 16). (C) PCA of sample distribution according to cluster frequency from B. Small circles: individual samples; big circles: mean of distribution.

Colors of the arrows and of the cluster labels reflect the relative contribution to the PCA. (D) Median and IQR of PhenoGraph cluster frequencies. Bars: SD. Dots:

single patient values. Two-sided Mann-Whitney test. (E) Representative flow cytometry of CD25+CD127- Tregs and (F) of their markers. Conventional CD4+CD25-

CD127+ T cells (Tconv) are depicted as a control. Numbers indicate the percentage of gated cells (E) or the MFI of marker expression. cDC, conventional dendritic

cell; CTL, cytotoxic T lymphocyte; iCCA, intrahepatic cholangiocarcinoma; MAIT, mucosal-associated invariant T; MFI, median fluorescence intensity; NK, natural

killer; PBMCs, peripheral blood mononuclear cells; PCA, principal component analysis; pDC, plasmacytoid dendritic cell; TCM, central memory T; Tconv, con-

ventional T cell; T EM, effector memory T; Treg, regulatory CD4+ T cell; T RM, tissue-resident memory T cell; T TE , terminal effector T; UMAP, uniform manifold

approximation and projection

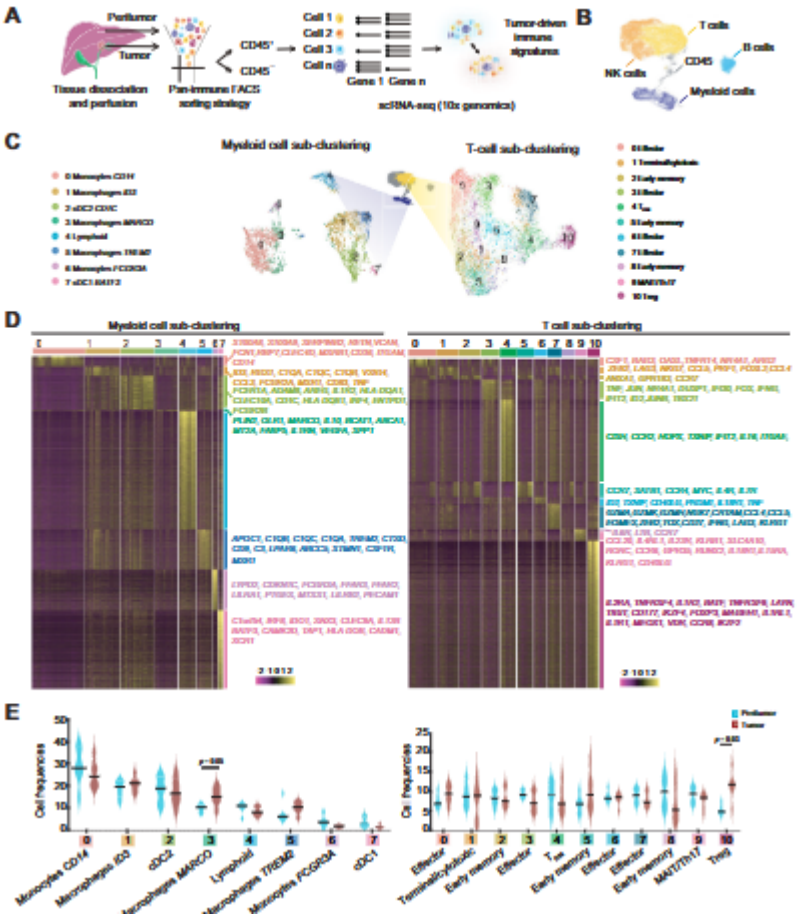


Fig. 2. Tumor-infiltrating leukocyte gene expression in iCCA by scRNA-seq.

(A) Experimental workflow (scRNA-seq of paired peritumoral and tumoral samples; n = 6). (B) UMAP of all cells (n = 31,745). (C) Colored clusters of T (n = 12,644) and myeloid cells (n = 4,585) visualized by UMAP. (D) Heatmap of marker genes in scRNA-seq clusters. Columns: single cells. Rows: cluster marker genes. Representative genes that are differentially expressed are on the right. (E) Violin plots showing the relative distribution of each T and myeloid cell cluster between tumoral and peritumoral samples. Lines: median frequencies. 2-way ANOVA test. NK, natural killer; cDC, conventional dendritic cell; MAIT, mucosal-associated invariant T;

scRNA-seq: single cell RNA-sequencing; TRM, tissue resident memory T; Th17, CD4+ T helper type-17; Treg, regulatory CD4+ T.

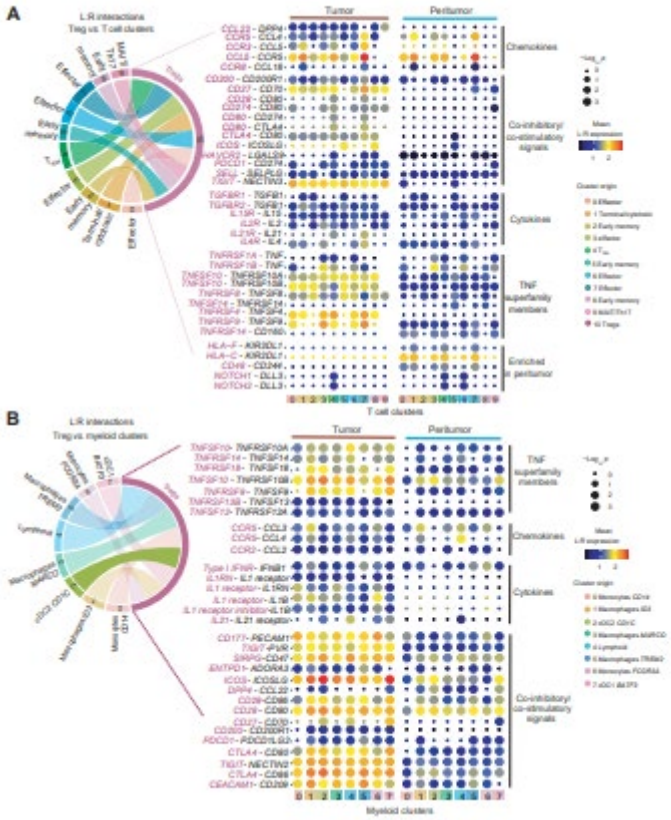


Fig. 3. Dynamic remodeling of the Treg interactome in iCCA.

CellPhoneDB intercellular communication analysis between Tregs (scRNA-seq cluster 10) and (A) T-cell or (B) myeloid cell clusters identified by scRNA-seq. In both A and B, circos plot show all predicted cell–cell interaction events via ligand:receptor (L:R) pairs, while bubble plots indicate the mean L:R expression (color scale) and the corresponding p value (size of the bubble). Molecules expressed by Tregs and the interacting populations are in purple and in black, respectively. cDC, conventional dendritic cell; MAIT, mucosal-associated invariant T; P: empirical permutation p value. Treg, regulatory CD4+ T; Th17, CD4+ T helper type-17; TRM, tissue resident memory T; TNF, tumor necrosis factor.

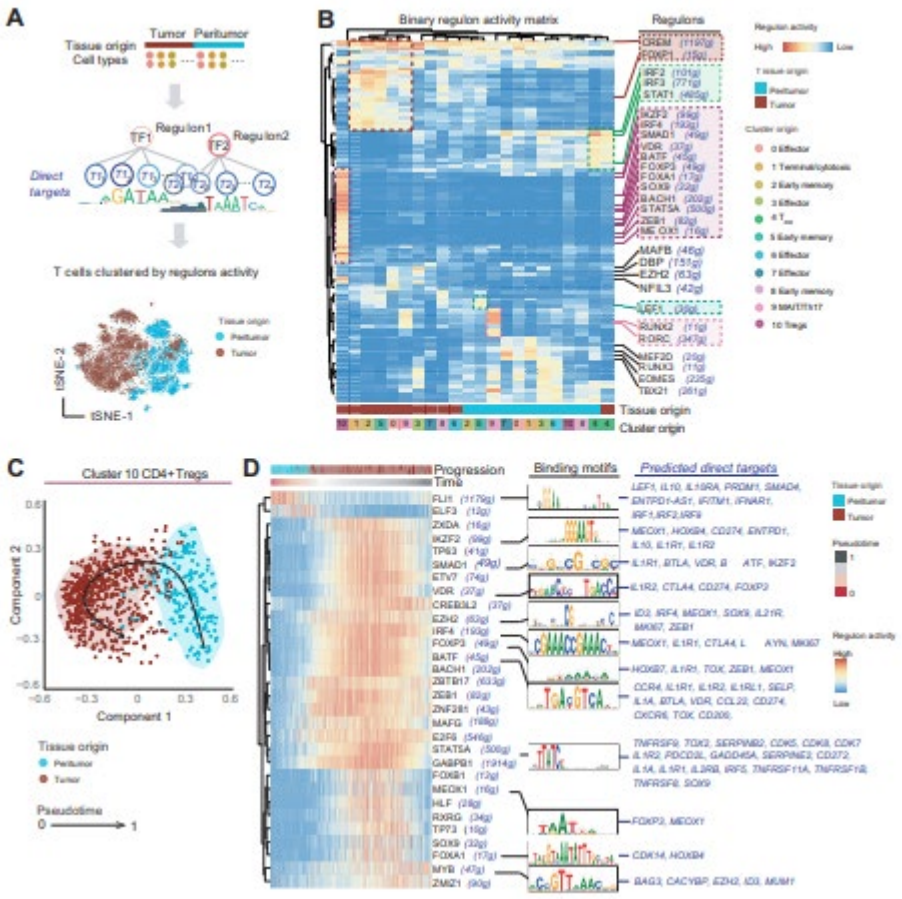


Fig. 4. Transcriptional network inference of iCCA-infiltrating T cells. (A) Top: SCENIC pipeline. Bottom: t-SNE map of T cells based on SCENIC regulon activity

scores. (B) Regulon activity heatmap in scRNA-seq T-cell clusters. Relevant transcription factors and the putative number of genes they regulate are indicated.

Colored dashed boxes: T-cell clusters with the highest regulon activities. (C) SCORPIUS trajectory map of CD4+ Tregs (scRNA-seq cluster 10) according to regulon

activity scores. (D) Pseudo-time (SCORPIUS) of regulon activity in single Tregs. The top 30 regulons leading the timeline, their DNA binding motifs and their

predicted targets (manually selected) are indicated. MAIT, mucosal-associated invariant T; Treg, regulatory CD4+ T; Th17, CD4+ T helper type-17; TRM, tissue

resident memory T; t-SNE, t-distributed stochastic neighbor embedding; TF, transcription factor.

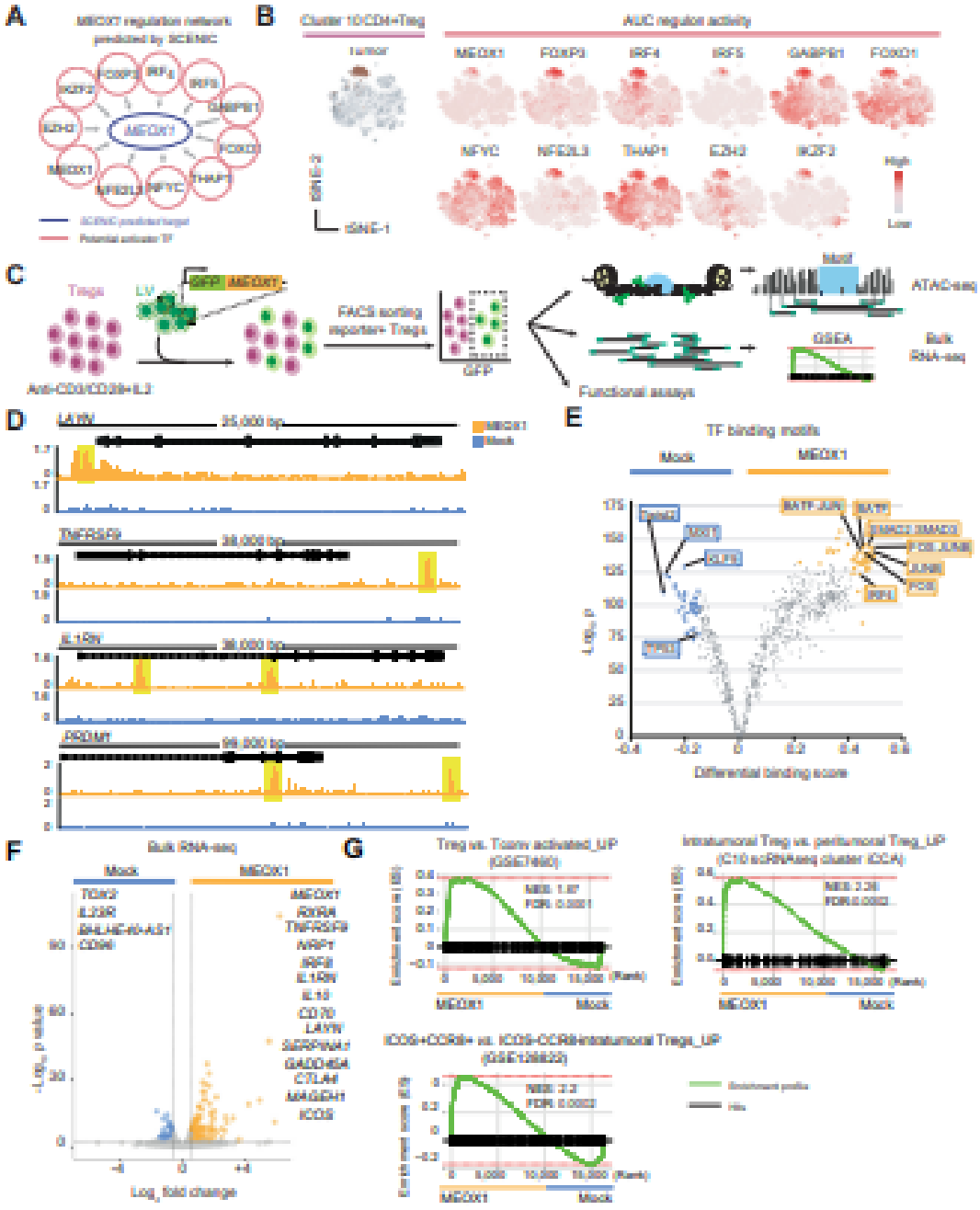


Fig. 5. MEOX1 reprograms Tregs to a tumor-infiltrating phenotype. (A) MEOX1 regulation network predicted by SCENIC. (B) t-SNE map of all T cells depicting

Tregs from tumors (scRNA-seq cluster 10) and regulons activating MEOX1 (predicted). (C) Experimental workflow of MEOX1 overexpression in circulating Tregs

(n = 3). (D) Representative differentially accessible genomic regions as from ATAC-seq (highlighted in yellow). (E) TF binding motif enrichment by TOBIAS

(significant motifs are colored). (F) Volcano plot of differentially expressed genes (bulk RNA-seq). Genes of interest are indicated. (G) GSEA of different gene sets in

bulk RNA-seq data obtained as in C. ATAC-seq, assay for transposase-accessible chromatin using sequencing; GSEA, gene set enrichment analysis; iCCA, intrahepatic cholangiocarcinoma; Tconv, conventional CD4+ T; TF, transcription factor; Treg, regulatory CD4+ T; t-SNE, t-distributed stochastic neighbor embedding.

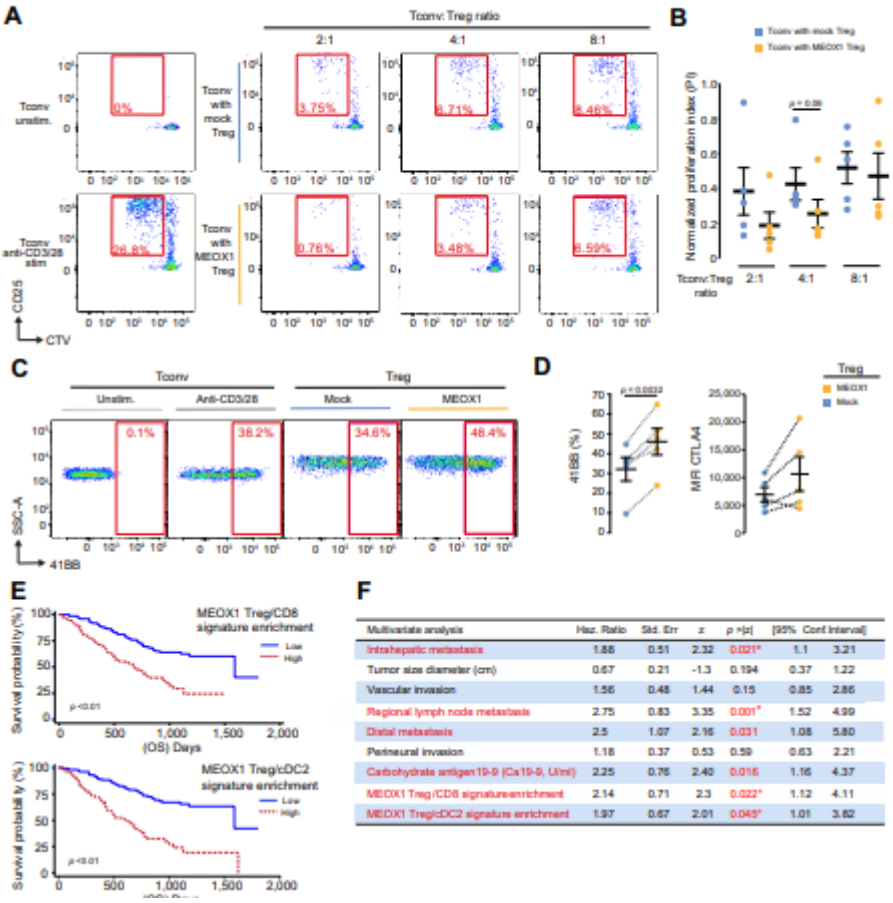


Fig. 6. MEOX1 upregulates 41BB in Tregs and defines a signature of iCCA progression. (A) Suppressive capacity of MEOX1 and mock-transduced Tregs on

Tconv. Numbers: percentage of proliferating cells. (B) Summary of the PI (mean ± SEM, n = 5), normalized by the PI of Tconv without Tregs. Paired t-test. (C)

Representative 41BB expression after 16h stimulation with Dynabeads. Unstimulated Tconv: staining control. (D) Summary of 41BB and CTLA4 expression (mean

± SEM; n = 5 independent experiments) by MEOX1 and mock-transduced Tregs. Paired t- test. (E) Kaplan-Meier OS curves (n = 147). (F) Multivariate coxregression analysis considering clinicopathological factors that were associated with OS in univariate analysis. cDC, conventional dendritic cell; MFI, median

fluorescence intensity; OS, overall survival; PI, proliferation index; Tconv, conventional CD4+ T; Treg, regulatory CD4+ T.